IEEE Access
Multidisciplinary ⋮ Rapid Review ⋮ Open Access Journal

Received February 18, 2021, accepted March 8, 2021, date of publication March 18, 2021, date of current version April 2, 2021.

Digital Object Identifier 10.1109/ACCESS.2021.3067108

Upper-Limb Kinematic Parameter Estimation and Localization Using a Compliant Robotic Manipulator

FRANCISCO J. RUIZ-RUIZ[1], JUAN M. GANDARIAS[2], (Member, IEEE), FRANCISCO PASTOR[1], AND JESÚS M. GÓMEZ-DE-GABRIEL[1], (Member, IEEE)

[1]Robotics and Mechatronics Group, University of Málaga, 29071 Málaga, Spain
[2]Human-Robot Interfaces and Physical Interaction Lab (HRI[2]), Istituto Italiano di Tecnologia (IIT), 16163 Genoa, Italy

Corresponding author: Francisco J. Ruiz-Ruiz (fjruiz2@uma.es)

This work was supported in part by the Spanish Projects under Grant UMA CEIATECH-23, Grant RTI2018-093421-B-I00, and Grant FEDER 2018 EQC2018-004299-P, and in part by the University of Málaga.

ABSTRACT Assistive and rehabilitation robotics have gained momentum over the past decade and are expected to progress significantly in the coming years. Although relevant and promising research advances have contributed to these fields, challenges regarding intentional physical contact with humans remain. Despite being a fundamental component of assistive and rehabilitation tasks, there is an evident lack of work related to robotic manipulators that intentionally manipulate human body parts. Moreover, existing solutions involving end-effector robots are not based on accurate knowledge of human limb dimensions and their current configuration. This knowledge, which is essential for safe human–limb manipulation, depends on the grasping location and human kinematic parameters. This paper addresses the upper-limb manipulation challenge and proposes a pose estimation method using a compliant robotic manipulator. To the best of our knowledge, this is the first attempt to address this challenge. A kinesthetic-based approach enables estimation of the kinematic parameters of the human arm without integrating external sensors. The estimation method relies only on proprioceptive data obtained from a collaborative robot with a Cartesian impedance-based controller to follow a compliant trajectory that depends on human arm kinodynamics. The human arm model is a 2-degree of freedom (DoF) kinematic chain. Thus, prior knowledge of the arm's behavior and an estimation method enables estimation of the kinematic parameters. Two estimation methods are implemented and compared: i) Hough transform (HT); ii) least squares (LS). Furthermore, a resizable, sensorized dummy arm is designed for experimental validation of the proposed approach. Outcomes from six experiments with different arm lengths demonstrate the repeatability and effectiveness of the proposed methodology, which can be used in several rehabilitation robotic applications.

INDEX TERMS Human–robot interaction, motion analysis, robot motion, assistive robotics.

I. INTRODUCTION

Assistive robots can be defined as devices equipped with sensory, perceptive, and cognitive capabilities to physically help disabled or elderly people in daily-life activities, thus circumventing the need for an attendant [1]. Typical existing applications involving this technology include activities that do not require high levels of physical interaction, such as feeding [2] or dressing [3]. However, the ability to facilitate tasks that involve high levels of physical interaction, such as climbing stairs or standing up from a bed or chair [4], relocating limbs [5], object handovers [6], and stabilizing limb motions [7], is also desired in assistive robots.

These physical assistance devices can also be employed in other fields, such as rehabilitation robotics, which has gained importance in recent years [8]. This field of robotics offers multiple benefits by improving treatment quality in terms of repeatability and efficiency and providing an objective approach to evaluate patients' progress [9]–[12].

One of the main challenges in physical robotic attendance and rehabilitation is the manipulation of human limbs [13]–[15]. In previous studies, this challenge has been addressed using two main approaches: exoskeletons and end-effector devices. Exoskeletons have been extensively studied and used for both assistance and rehabilitation purposes.

The associate editor coordinating the review of this manuscript and approving it for publication was Luigi Biagiotti.

These systems are wearable devices designed for multiple purposes. Some of the applications include helping patients in their daily tasks (e.g., suppressing upper limb tremors in people with neurological damage [16]), assisting people with heavy loads [17], and rehabilitation (e.g., the hand and wrist rehabilitation robots described in [18] and [19]). However, these systems are usually heavy, obtrusive, and difficult to wear. In contrast, end-effector systems, although bulky, tend to be multipurpose. This solution can be implemented using collaborative robot arms (Cobots), sensitive manipulators, or industrial manipulators with external force/torque sensors [20], [21]. One of the main advantages is that these systems are not attached to the human body; hence, the same system can be used for multiple tasks, especially if the system is mounted on a mobile platform [22]. Regarding rehabilitation applications, end-effector robots are used under a therapist's supervision and have been successfully implemented for upper-limb tremor suppression [7]. In addition to these two approaches, a few ad hoc solutions based on custom-designed devices with unique mechanical configurations have been considered [23], [24]. One of the main advantages of these solutions is that they provide more efficient or safer functionality for specific tasks [25].

This work focuses on the application of compliant, end-effector manipulator systems for rehabilitation tasks. Sensitive manipulators include joint torque sensors that can be used to provide compliant control schemes in the task space. Cartesian impedance control in robots used for human interactions enables the robot to adapt to physical contact with the user. In this respect, low impedance ensures more compliant robot behavior but can cause poor task performance in terms of movement accuracy and precision. In contrast, a high impedance improves the programmed task's performance but can compromise user safety. Nevertheless, in the works cited above, the robotic systems do not adopt an active manipulative role; i.e., the robots do not directly manipulate human limbs but adapt to the motion intended by the human. During direct manipulation of human body parts, the use of a stand-alone compliant controller is not sufficient to ensure safety; more information is needed. In this respect, an accurate kinodynamic model of the human subject and real-time monitoring of the joint pose of the subject lead to several improvements in performance, safety and precision.

Existing approaches include visual methods for estimating human posture [26], [27]. However, due to several limitations (e.g., camera placement, illumination settings, or occlusions), such methods are not sufficiently accurate and robust for daily-life activities with critical safety restrictions. To overcome this problem, a combination of optical [28], [29] and inertial [30], [31] sensors is typically employed. These solutions involve computationally expensive algorithms that must be executed concurrently with the application. Consequently, synchronization between the two systems is essential for accomplishing the task.

A different approach consists of the use of proprioceptive information. A robot can obtain the human subject kinodynamic model from the resultant trajectories of the physical human–robot interaction (pHRI) task. Based on this concept, a method that estimates the link weights in human upper limbs to compensate for the gravitational forces of exoskeletons has recently been presented [32]. Laitenberger *et al.* proposed a method to estimate the parameter values using offline external tools [33]. Moreover, recent developments in robot sensing for pHRI include the use of underactuated grippers equipped with tactile sensing and kinesthetic (position) perception to improve their knowledge of grasped objects [34] and estimation of the roll angle of the grasped human forearm with an underactuated gripper [5]. Based on the same principle, the compliant robot's resulting trajectories during the manipulation of a human limb can be used as individual-specific data to estimate the limb's kinematic parameters and poses.

This study contributes to the human-limb robotic manipulation problem by addressing the challenge of upper-limb parameter estimation with a commercial robot arm using kinesthetic information only. In this paper, we propose a novel approach that requires only a simple ascendant motion to estimate the kinematic parameters of a passive person's arm. To the best of the authors' knowledge, this study represents the first and only work in this domain. The proposed method enables estimation of the human arm kinematic model without the need for external sensors (e.g., cameras, mocaps). Motion planning algorithms can then be used along with the estimated model in multiple assistive and rehabilitation applications that require upper-limb manipulation. The estimated parameters include the distance from the grasping location to the elbow, the distance between the elbow and shoulder axes (humerus length), and the elbow and shoulder poses. This task requires a manipulator robot with Cartesian compliance control, a suitable gripper, and real-time position feedback. When no visual methods are used, the initial grasping of the human forearm is performed with the help of a human supervisor. Once the attachment is complete, the method is fully autonomous and does not require further supervision. To validate our approach, a 3D-printed, customizable, sensorized anthropomorphic arm is used. The dummy arm has 6 DoFs and a mass and length similar to those or a real human arm. Moreover, the dummy arm integrates joint sensors that provide ground-truth data.

The remainder of this paper is organized as follows: In Section II, we present the problem, its formulation, and constraints. Section III describes the proposed method. In Section IV, the experiments conducted to evaluate the system's performance under different kinodynamic conditions are presented. In Section V, we discuss the experimental results and the limitations of the proposed methodology. Finally, Section VI presents the conclusions and possible lines of future research.

II. PROBLEM STATEMENT

The challenge described above is simplified by assuming that the human arm is extended with the forearm section lying

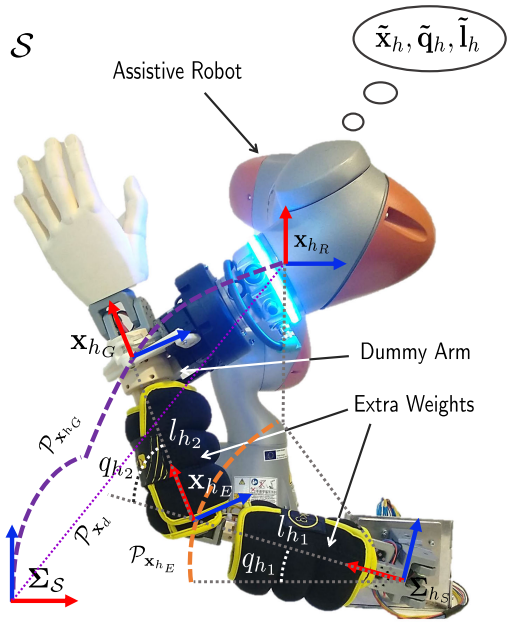

FIGURE 1. Illustration of the problem addressed in this work: A compliant robot manipulating a 3D-printed dummy arm that simulates the behavior of a human arm. Due to the compliance of the Cartesian impedance controller, the robot motion adapts to the kinodynamics of the dummy arm, modifying the end-effector trajectory and allowing the estimation of the kinematic parameters. The XYZ-RGB convention has been applied in all reference frames. A full description of the parameters can be found in Section II.

on a surface, as typically observed in various rehabilitation tasks [35]–[37]. Considering the scenario illustrated in Fig. 1, a compliant robot grasps the arm to manipulate it in a specific way based on the desired task. During the manipulation, the robot may perform motions in the human-arm task space causing the arm to reach dangerous configurations in the joint space and, therefore, injuring the subject. Examples of unsafe movements include those that exceed the joint range or cause the elbow to hit nearby surfaces (e.g., floor, bed, stretcher), leading to possible physical injury for a vulnerable person (elderly, patient, or victim).

A. APPROACH

The proposed approach involves developing a method to identify the kinematic parameters of a human upper limb for pose estimation and safe manipulation with a compliant robot, considering the robot does not have any previous information about these parameters. This method is based on implementing an estimation trajectory before the desired assistive or rehabilitation task. Once the motion is initiated, the robot can use an estimated kinematic model to limit the workspace and plan motions according to the task requirements and safety restrictions.

A schematic of the problem is shown in Fig. 1, where all the geometric elements are represented in the human sagittal plane ($\mathcal{S}$). The subscript h refers to the human arm, with $\mathbf{x}_{h_G}$, $\mathbf{x}_{h_E}$, and $\mathbf{x}_{h_S} \in \mathbb{R}^3$ representing the pose (position $\in \mathbb{R}^2$ and orientation $\in \mathbb{R}$) of the grasping point, elbow, and shoulder, respectively. For clarity, the XYZ-RGB convention is used in all figures in this paper. Hence, the axis labels of the reference frames are omitted.

Another assumption involved in our proposal is that the human subject is considered entirely passive (i.e., an unconscious person or a relaxed, collaborative patient) during the estimation motion. In a real-world scenario, a supervisor or therapist should ask the patient to remain still while the robot is performing the estimation trajectory. Hence, the torques at the human arm joints are null ($\boldsymbol{\tau}_h = 0$). Therefore, all wrenches applied to the human arm originate from the gravitational forces of the arm and the motion of the robot manipulator. The robot has an impedance-based controller (explained in Section III-B), which ensures compliant motion when the robot moves the human arm in $\mathcal{S}$ while restricting the motion out of this plane. This compliance causes the trajectory of the end-effector to change due to the dynamic effects and kinematic constraints of the human arm. Then, when the desired path $\mathcal{P}_{\mathbf{x}_d}$ is to be followed, the kinodynamics of the human arm modify this path, and the end-effector follows the actual path $\mathcal{P}_{\mathbf{x}_{h_G}}$.

Thus, the main idea of this approach is that the actual, modified path $\mathcal{P}_{\mathbf{x}_{h_G}}$ can be used to estimate the parameters of an identification model (Υ). These parameters are the lengths of the human forearm and upper arm ($\mathbf{l}_h \in \mathbb{R}^2$) and the reference frame of the shoulder ($\boldsymbol{\Sigma}_{h_S}$) with respect to the grasping point in the sagittal plane reference frame ($\boldsymbol{\Sigma}_{\mathcal{S}}$), given by

$$\left[\tilde{\mathbf{l}}_h, \tilde{\Sigma}_{h_S}\right] = \Upsilon\left(\mathcal{P}_{\mathbf{x}_{h_G}}\right). \tag{1}$$

Here, the symbol ($\tilde{}$) refers to the estimated parameters. This model is explained in detail in Section III-C.

B. HUMAN ARM DYNAMICS

In pHRI applications, the analysis of interaction wrenches is crucial for developing a safety system [38]. Such an analysis is even more critical in complex human-limb manipulation applications. In this section, the human arm's dynamic model is described, and the wrenches involved in the interaction between the arm and the robot during the estimation movement are analyzed. According to [39], the human arm can be modeled as a 7-DoF manipulator. When manipulating the arm, the robotic manipulator's acceleration and velocity are low due to safety requirements. Hence, under this assumption, the inertial and Coriolis effects that the robot motion produces on the human arm joint space are reduced. Therefore, the dominant dynamic effects are gravitational. No additional kinematic information about the human arm is acquired when performing motions outside of plane $\mathcal{S}$. Hence, in this study, the task space is limited to the plane $\mathcal{S}$. This constraint is one of the main limitations of the proposed method and is discussed in more detail in Section V.

An impedance Cartesian controller can restrict the task space of the human arm to the plane $\mathcal{S}$ if the axis's impedance perpendicular to the plane and the respective rotational impedance indexes are sufficiently high (see Section III-B).

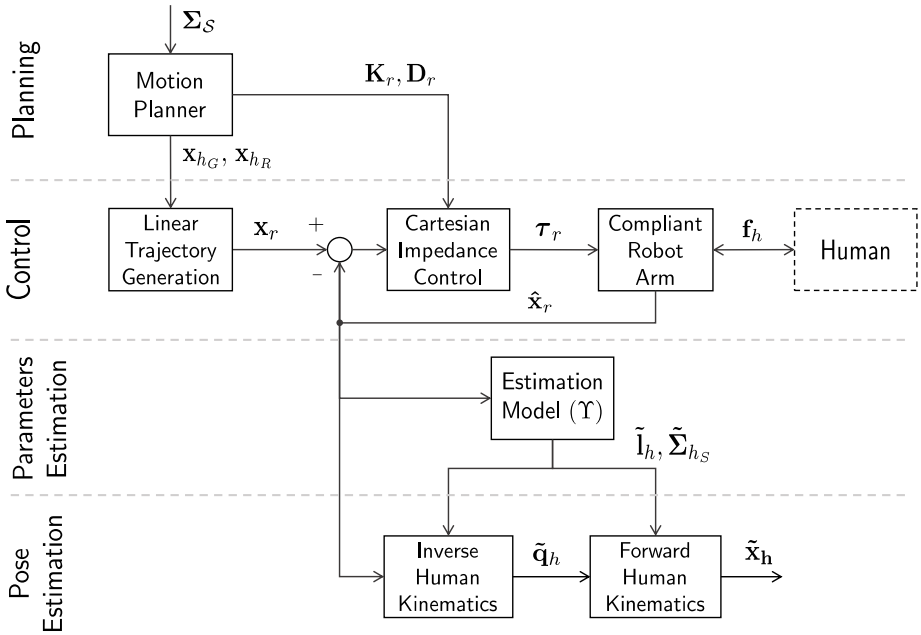

FIGURE 2. Schematic of the proposed approach, divided into four stages: i) planning; ii) control; iii) parameter estimation; iv) pose estimation.

Hence, the following simplification can be considered: the human arm's dynamic behavior, which establishes the dynamic relationships between the human-arm task and joint spaces, can be modeled as a simplified 2-DoF manipulator contained in the sagittal plane, as shown below.

$$\underbrace{\mathbf{M}_h(\mathbf{q}_h)\,\ddot{\mathbf{q}}_h}_{\ll \mathbf{g}_h(\mathbf{q}_h)} + \underbrace{\mathbf{C}_h(\mathbf{q}_h, \dot{\mathbf{q}}_h)\,\mathbf{q}_h}_{\ll \mathbf{g}_h(\mathbf{q}_h)} + \mathbf{g}_h(\mathbf{q}_h) = \underbrace{\boldsymbol{\tau}_h}_{0} + \mathbf{J}_h^T(\mathbf{q}_h)\,\mathbf{f}_h, \tag{2}$$

where $\mathbf{q}_h \in \mathbb{R}^2$ defines the joint space configuration, $\mathbf{M}_h \in \mathbb{R}^{2\times2}$ is the symmetric and positive mass matrix, $\mathbf{C}_h \in \mathbb{R}^{2\times2}$ is the Coriolis matrix, $\mathbf{g}_h \in \mathbb{R}^2$ and $\boldsymbol{\tau}_h \in \mathbb{R}^2$ are the gravity and torque vectors, respectively, $\mathbf{J}_h^T \in \mathbb{R}^{2\times2}$ is the Jacobian matrix, and $\mathbf{f}_h \in \mathbb{R}^3$ is the interaction force vector of the human arm.

As defined by (2), the most significant dynamic effects on the human arm during the estimation motion are gravitational; thus, no damage is caused to the human arm joints due to the applied wrenches. Similarly, the impedance-based controller, which defines the dynamic robotic behavior, ensures that the human-arm joint space limits are not violated. Details regarding the motion planning and Cartesian impedance controller are provided in Sections III-A and III-B, respectively.

III. LIMB ESTIMATION METHOD

This section describes the four structural elements of the architecture shown in Fig. 2: i) planning, ii) control, iii) parameter estimation, and iv) pose estimation.

A. MOTION PLANNING

At the beginning of the operation, the robot's end-effector is located at $\mathbf{x}_{h_G}$. This point can be set by an operator or autonomously calculated by the robot using computer vision techniques, such as the one presented in [40]. However, the performance of these methods is sensitive to the lighting conditions. Moreover, possible occlusions caused by clothes or bed sheets may render these methods ineffective. Nevertheless, the method to obtain $\mathbf{x}_{h_G}$ is beyond the scope of this work. The proposed approach is based on common robotic rehabilitation procedures [41], in which the gripper is manually placed by a human supervisor (therapist). Once the gripper grasps the arm, the center of the grasp and its orientation are recorded; thus, $\mathbf{\Sigma}_\mathcal{S}$ is set. Similarly, the sagittal plane, which is the vertical plane that contains the gripper XZ-axis, is also obtained. For convenience, the XZ-coordinates are taken as the coordinates of $\mathcal{S}$ (see Section IV-B).

To identify the kinematic parameters, the manipulator must perform the following operation (see Fig. 1): at the beginning of the operation, the human arm is placed on a flat surface (e.g., a bed or a table), and the gripper grasps the wrist at $\mathbf{x}_{h_G}$. Then, a trajectory command to move the arm from $\mathbf{x}_{h_G}$ to a point ($\mathbf{x}_{h_R} \in \mathbb{R}^3$) is transmitted to the robot. This point is precomputed from $\mathbf{x}_{h_G}$ considering the initial joint position of the human arm with $q_{h_0} = 0$, final joint position $q_{h_f} = \pi/4$, and length $l_{h_0} = 300\,mm$. Then, $\mathbf{x}_{h_R}$ is computed as follows:

$$\mathbf{x}_{h_R} = \begin{bmatrix} x_{h_G} + l_{h_0}\left(\cos\left(q_{h_f}\right) + 1\right) \\ z_{h_G} + l_{h_0}\left(\sin\left(q_{h_f}\right) + 1\right) \\ \psi_{h_G} + \frac{\pi}{2} \end{bmatrix}. \tag{3}$$

The robot tries to follow a linear interpolation path $\left(\mathcal{P}_{\mathbf{x}_d}\right)$ between $\mathbf{x}_{h_G}$ and $\mathbf{x}_{h_R}$ (see Fig. 1). The actual path $(\mathcal{P}_{\mathbf{x}_{h_G}})$ depends on the human arm parameters, such as the link weights and lengths. $\mathbf{x}_{h_G}$ is used to identify the kinematic parameters using two estimation methods: the generalized Hough transform (HT) [42] and the least squares method (LS) (see Section III-C).

B. ROBOT CONTROL

The estimation must be conducted under an impedance control scheme to ensure that the robot follows a path within the natural human arm range of motion. This section describes the employed impedance controller. We consider the dynamic model of a generic n-DoF manipulator, which is defined as follows:

$$\mathbf{M}_r(\mathbf{q}_r)\ddot{\mathbf{q}}_r + \mathbf{C}_r(\mathbf{q}_r, \dot{\mathbf{q}}_r)\dot{\mathbf{q}}_r + \mathbf{g}_r(\mathbf{q}_r) = \boldsymbol{\tau}_r + \boldsymbol{\tau}_{r_{ext}}, \quad (4)$$

where the subindex r refers to the robotic manipulator, $\mathbf{q}_r \in \mathbb{R}^n$ defines the joint space configuration, $\mathbf{M}_r(\mathbf{q}_r) \in \mathbb{R}^{n\times n}$ is the symmetric and positive mass matrix, $\mathbf{C}_r(\mathbf{q}_r, \dot{\mathbf{q}}_r) \in \mathbb{R}^{n\times n}$ is the Coriolis matrix, $\mathbf{g}_r(\mathbf{q}_r) \in \mathbb{R}^n$ and $\boldsymbol{\tau}_r \in \mathbb{R}^n$ are the gravity and input torque vectors, respectively, and $\boldsymbol{\tau}_{r_{ext}} \in \mathbb{R}^n$ is the external torque vector.

Although the proposed estimation methodology is valid for both redundant and nonredundant manipulators, the former type with seven DoFs ($n = 7$) was used in this study, and the impedance controller described below is the same type. Impedance controllers for nonredundant manipulators are described in [43]. To design a Cartesian impedance controller for a redundant manipulator, an end-effector dynamic model in the operational space [44] is required:

$$\boldsymbol{\Lambda}_r(\mathbf{q}_r)\ddot{\mathbf{x}}_r + \boldsymbol{\mu}_r(\mathbf{q}_r, \dot{\mathbf{q}}_r)\dot{\mathbf{x}}_r + \mathbf{f}_{r_g}(\mathbf{q}_r) = \mathbf{f}_r + \mathbf{f}_{r_{ext}}, \quad (5)$$

where $\mathbf{x}_r \in \mathbb{R}^6$ is the task coordinate vector in Cartesian space, $\boldsymbol{\Lambda}_r(\mathbf{q}_r) \in \mathbb{R}^{6\times6}$ is the end-effector inertia matrix, $\boldsymbol{\mu}_r(\mathbf{q}_r, \dot{\mathbf{q}}_r) \in \mathbb{R}^{6\times6}$ is the Cartesian Coriolis matrix, and $\mathbf{f}_{r_g}(\mathbf{q}_r) = \mathbf{J}_r^{\dagger T}(\mathbf{q}_r)\mathbf{g}_r(\mathbf{q}_r) \in \mathbb{R}^6$, $\mathbf{f}_r = \mathbf{J}_r^{\dagger T}(\mathbf{q}_r)\boldsymbol{\tau}_r \in \mathbb{R}^6$, and $\mathbf{f}_{r_{ext}} \in \mathbb{R}^6$ are the gravitational, control, and external forces vectors, respectively. Notably, only the end-effector dynamics are considered in (5); the null-space dynamics are not included. The matrix $\mathbf{J}^\dagger(\mathbf{q}_r)$ is the dynamically consistent generalized inverse of the Jacobian matrix, which is defined as

$$\mathbf{J}_r^\dagger(\mathbf{q}_r) = \mathbf{M}_r^{-1}(\mathbf{q}_r)\mathbf{J}_r^T(\mathbf{q}_r)\left(\mathbf{J}_r(\mathbf{q}_r)\mathbf{M}_r^{-1}(\mathbf{q}_r)\mathbf{J}_r^T(\mathbf{q}_r)\right)^{-1} \quad (6)$$

The end-effector inertia matrix $\boldsymbol{\Lambda}_r(\mathbf{q}_r)$ and the Cartesian Coriolis matrix $\boldsymbol{\mu}_r(\mathbf{q}_r, \dot{\mathbf{q}}_r)$ can be computed as in [45]:

$$\boldsymbol{\Lambda}_r(\mathbf{q}_r) = \left(\mathbf{J}_r(\mathbf{q}_r)\mathbf{M}_r^{-1}(\mathbf{q}_r)\mathbf{J}_r^T(\mathbf{q}_r)\right)^{-1}, \quad (7)$$

$$\boldsymbol{\mu}_r(\mathbf{q}_r, \dot{\mathbf{q}}_r)\dot{\mathbf{x}}_r = \boldsymbol{\Lambda}_r(\mathbf{q}_r)\Big(\boldsymbol{J}_r(\mathbf{q}_r)\mathbf{M}_r^{-1}(\mathbf{q}_r)\mathbf{C}_r(\mathbf{q}_r, \dot{\mathbf{q}}_r) - \dot{\mathbf{J}}_r(\mathbf{q}_r)\Big)\dot{\mathbf{q}}_r. \quad (8)$$

During the estimation movement, the desired robot behavior is similar to that of a mass–spring–damper system:

$$\boldsymbol{\Lambda}_d\ddot{\mathbf{x}}_e + \mathbf{D}_r\dot{\mathbf{x}}_e + \mathbf{K}_r\mathbf{x}_e = \mathbf{f}_{r_{ext}}, \quad (9)$$

where $\mathbf{x}_e = \mathbf{x}_r - \mathbf{x}_d$ is the position error between the robot position $\mathbf{x}_r$ and the desired virtual equilibrium position $\mathbf{x}_d$; and $\boldsymbol{\Lambda}_d \in \mathbb{R}^{6\times6}$, $\mathbf{D}_r \in \mathbb{R}^{6\times6}$, and $\mathbf{K}_r \in \mathbb{R}^{6\times6}$ are the desired inertia, damping, and stiffness matrices of the end-effector, respectively. $\boldsymbol{\Lambda}_d$, $\mathbf{K}_r$, and $\mathbf{D}_r$ are constant, symmetric positive-definite matrices.

For simplicity, the desired end-effector inertia matrix is set as identical to the robot end-effector inertia matrix, $\boldsymbol{\Lambda}_d = \boldsymbol{\Lambda}_r(\mathbf{q}_r)$. In addition, to ensure the passivity and stability of the system with a time-varying inertia matrix, the Coriolis matrix must be included. The stability proof of that argument is developed in detail in [46]. Thus, equation (9) can be rewritten as

$$\boldsymbol{\Lambda}_r(\mathbf{q}_r)\ddot{\mathbf{x}}_e + (\boldsymbol{\mu}_r(\mathbf{q}_r, \dot{\mathbf{q}}_r) + \mathbf{D}_r)\dot{\mathbf{x}}_e + \mathbf{K}_r\mathbf{x}_e = \mathbf{f}_{r_{ext}}. \quad (10)$$

Moreover, as the end-effector inertia matrix depends on the end-effector pose, the damping matrix should not be constant for the same reason as mentioned above. A robot pose-dependent damping matrix is defined in [47].

Therefore, the desired robot behavior can be achieved by the following control law:

$$\mathbf{f}_{r_{ext}} = \mathbf{f}_{r_g}(\mathbf{q}_r) + \boldsymbol{\Lambda}_r(\mathbf{q}_r)\ddot{\mathbf{x}}_d + \boldsymbol{\mu}_r(\mathbf{q}_r, \dot{\mathbf{q}}_r)\dot{\mathbf{x}}_d - \mathbf{D}_r(\mathbf{q}_r)\dot{\mathbf{x}}_e - \mathbf{K}_r\mathbf{x}_e. \quad (11)$$

The input torque of the Cartesian impedance controller is then defined as

$$\boldsymbol{\tau}_r = \mathbf{g}(\mathbf{q}_r) + \mathbf{J}_r^T(\mathbf{q}_r)(\boldsymbol{\Lambda}_r(\mathbf{q}_r)\ddot{\mathbf{x}}_d + \boldsymbol{\mu}_r(\mathbf{q}_r, \dot{\mathbf{q}}_r)\dot{\mathbf{x}}_d - \mathbf{D}_r(\mathbf{q}_r)\dot{\mathbf{x}}_e - \mathbf{K}_r\mathbf{x}_e). \quad (12)$$

Thus, by assuming that the interaction wrenches with the human arm are the only ones applied to the manipulator during the estimation, we can state that $\mathbf{f}_{r_{ext}} = \mathbf{f}_h$. In addition, once the robot grasps the arm on $\mathbf{x}_{h_G}$, we can assume that $\hat{\mathbf{x}}_r = \mathbf{x}_{h_G}$ during the entire manipulation process, and this is true only when the grasping is stable. In this study, zero slippage and a stable grasp during the entire manipulation process were considered because this problem is not a part of this work and should be considered separately.

C. PARAMETER ESTIMATION

Once the task, controller, and motion planning are set, multiple methodologies can be used to obtain an estimation model Υ [48]. This works uses and compares the performance of the HT and LS approaches.

a: HOUGH TRANSFORM

HT is a feature extraction technique used in computer vision that was primarily designed for line detection [49], although it is also capable of identifying any arbitrary curve. It is based on a voting procedure performed in parametric space ($\mathbb{P}$), through which candidates are obtained as local maxima in the accumulator space ($\mathbb{A}$). We know that $\mathbf{x}_{h_G}$ and $\mathbf{x}_{h_E}$ describe circumferences with centers in $\mathbf{x}_{h_E}$ and $\mathbf{x}_{h_S}$, respectively. These circumferences ($\mathcal{C}$) are defined by

$$\mathcal{C}\{r, s, t\} \equiv (x_{h_G} - s)^2 + (z_{h_G} - t)^2 = r^2, \quad (13)$$

where r denotes the radius and s and t are the coordinates of the center in $\mathcal{S}$, respectively. Then, we define the accumulator matrix ($\mathbf{A} \in \mathbb{N}^{\rho\times\sigma\times\varsigma}$) as

$$\mathbf{A} = \quad , \tag{14}$$

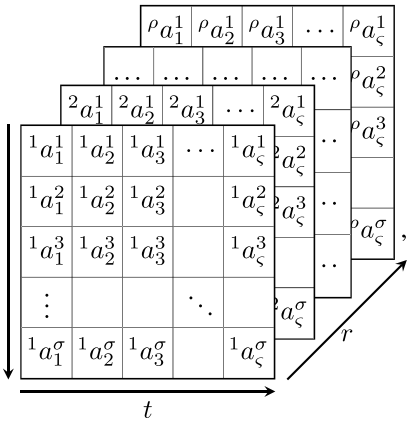

where ρ, σ, and $\varsigma \in \mathbb{N}$ are the maximum numbers of possible values of r, s, and t, respectively. Each element ${}^{r}a_{s}^{t}$ of $\mathbf{A}$ accumulates votes for a certain circumference of the i-th observation.

$$ {}^{r}a_{s}^{t} = \sum_{i=1}^{N} \mathcal{C}\left\{r, s, t\right\}, \tag{15}$$

where N is the total number of observations, defining all possible circumferences in the parameter space ($\mathbb{P} = \{(r, s, t)$, with $s,\ t \in \mathbb{Z},\ r \in \mathbb{N}\}$).

Because each point of the path can fit an infinite number of circumferences, the following assumptions are made to reduce the search volume and computational load:

1) $\mathcal{S}$ has been discretized with a 1 mm grid:
$$s,\ t \in \mathbb{Z}, \quad r \in \mathbb{N}. \tag{16}$$
2) Considering the common lengths of the parts of the human arm, circumferences with radii greater than $\rho =$ 500 mm are disregarded:
$$s \in \left[x_{h_G} - \rho,\ x_{h_G} + \rho\right], \quad \sigma, \varsigma = 2\,\rho. \tag{17}$$
3) The centers of the circumferences are normal to the path of the end-effector:
$$t = z_{h_G} + \left(s - x_{h_G}\right)\ tan(\psi_{h_G}). \tag{18}$$

Based on these considerations, we can define the HT algorithm ($\mathcal{H}\left(\mathcal{P}_{\mathbf{x}}\right)$) described in Algorithm 1 for a certain path with N observations $\mathcal{P}_{\mathbf{x}} = \{\mathbf{x}_1, \ldots, \mathbf{x}_i, \ldots, \mathbf{x}_N\}$. This algorithm calculates the most voted curve $\mathcal{C}^*\{r^*, s^*, t^*\}$ and returns the radius of this curve (r^*), which is used to estimate the distances of the parts of the human arm.

Once the radius of the circumference is identified, the pose of its center ($\mathbf{x}_c$) can be computed with respect to a certain point $\mathbf{x}_i$ on the path, according to the function $\mathcal{F}\left(\mathbf{x}_i, r^*\right)$

$$\mathcal{F}\left(\mathbf{x}_i, r^*\right) \equiv \begin{cases} x_c = x_i - r^* \cdot cos(\psi_i) \\ z_c = z_i - r^* \cdot sin(\psi_i) \\ \psi_c = \arctan\left(\dfrac{\|z_c - z_i\|}{\|x_c - x_i\|}\right) \end{cases} \tag{19}$$

Therefore, the HT identification model can be defined as

$$\Upsilon_{HT}\left(\mathcal{P}_{\mathbf{x}_{h_G}}\right) \equiv \begin{cases} \tilde{l}_{h_2} = \mathcal{H}\left(\mathcal{P}_{\hat{\mathbf{x}}_r}\right) \\ \tilde{l}_{h_1} = \mathcal{H}\left(\mathcal{P}_{\tilde{\mathbf{x}}_{h_E}}\right) \\ \tilde{\mathbf{\Sigma}}_{h_S} = \mathcal{F}\left(\tilde{\mathbf{x}}_{h_E}, \tilde{l}_{h_1}\right), \end{cases} \tag{20}$$

Algorithm 1 $\mathcal{H}\left(\mathcal{P}_{\mathbf{x}}\right)$

```
Initialize A: A = 0
for i = 1: N do
  for s = x_i − ρ: x_i + ρ do
    Compute t: t (x_i, s) ← (18)
    Compute r: r (x_i, s, t) ← (13)
    if r ≤ ρ then
      Update A (r, s, t): ^r a_s^t = ^r a_s^t + 1
    end if
  end for
end for
Get C*: C* {r*, s*, t*} ← argmax_{r,s,t} A (r, s, t)
return r*
```

where the estimation of the elbow pose with respect to the grasping point is given by

$$\tilde{\mathbf{x}}_{h_e} = \mathcal{F}\left(\tilde{\mathbf{x}}_{h_G}, \tilde{l}_{h_2}\right). \tag{21}$$

b: LEAST SQUARES

LS is a standard approach widely used in regression analysis and parameter estimation [50]–[52]. LS optimizes the parameters of a model to best fit a data set by minimizing the sum of the squares of the residuals [53]. Let $\{(v_k, w_k)\}_{k=1}^{n}$ be a data set of n observations composed of a scalar output w_k and a vector input $v_k \in \mathbb{R}^m$ with $n > m$. Hence, the goal is to find a function $f\ (v)$ such that $f\ (v_k) \approx w_k$:

$$w_k = f\ (v_k) = u_1 v_1 + \cdots + u_m v_m. \tag{22}$$

Expanding (22) for the n observations of the data set, one obtains an overdetermined linear system that can be written in matrix form as

$$\mathbf{V}\boldsymbol{u} = \mathbf{W}, \tag{23}$$

where $\mathbf{V}$ is the coefficient matrix, $\boldsymbol{u}$ is the vector of unknowns, and $\mathbf{W}$ is the constant terms matrix. According to [54], the vector of unknowns $\boldsymbol{u}$ that minimizes the quadratic error is given by

$$\hat{\boldsymbol{u}} = \left(\mathbf{V}^T\mathbf{V}\right)^{-1}\mathbf{V}^T\mathbf{W} \tag{24}$$

As mentioned above, $\mathbf{x}_{h_G}$ and $\mathbf{x}_{h_E}$ describe a circumference. To estimate the parameters of such a circumference via the LS method, one should express (13) in a more appropriate form:

$$u_1 x_{h_G} + u_2 z_{h_G} - u_3 = x_{h_G}^2 + z_{h_G}^2, \tag{25}$$

where $u_1 = 2s$, $u_2 = 2t$ and $u_3 = \left(s^2 + t^2 - r^2\right)$. Evaluating (25) for the whole set of points of the path yields an overdetermined system of N linear equations and 3 unknowns, as shown in (23). Then, one can define the vector of unknowns $\boldsymbol{u} = [u_1, u_2, u_3]^T$, the coefficient matrix $\mathbf{V}$ and

the constant terms matrix $\mathbf{W}$ as:

$$\mathbf{V} = \begin{bmatrix} x_{h_{G1}} & z_{h_{G1}} & -1 \\ \vdots & \vdots & \vdots \\ x_{h_{GN}} & z_{h_{GN}} & -1 \end{bmatrix},$$
$$\mathbf{W} = \begin{bmatrix} x_{h_{G1}}^2 + z_{h_{G1}}^2 \\ \vdots \\ x_{h_{GN}}^2 + z_{h_{GN}}^2 \end{bmatrix}. \quad (26)$$

Thus, after obtaining $\boldsymbol{u}$ as in (24), the radius of the circumference that offers the best fit to the path is given by

$$r = \mathcal{LS}\left(\mathcal{P}_{\mathbf{x}}\right) = \sqrt{\left(\frac{u_1}{2}\right)^2 + \left(\frac{u_2}{2}\right)^2 - u_3}. \quad (27)$$

Once the radius is estimated, the position of its center can be obtained by (19). Hence, the LS identification model if defined as

$$\Upsilon_{LS}\left(\mathcal{P}_{\mathbf{x}_{h_G}}\right) \equiv \begin{cases} \tilde{l}_{h_2} = \mathcal{LS}\left(\mathcal{P}_{\hat{\mathbf{x}}_r}\right) \\ \tilde{l}_{h_1} = \mathcal{LS}\left(\mathcal{P}_{\tilde{\mathbf{x}}_{h_E}}\right) \\ \tilde{\boldsymbol{\Sigma}}_{h_S} = \mathcal{F}\left(\tilde{\mathbf{x}}_{h_E}, \tilde{l}_{h_1}\right), \end{cases} \quad (28)$$

where the estimation of the elbow pose is obtained by (21).

D. LIMB POSE ESTIMATION FOR SAFE MANIPULATION

Once the kinematic model parameters have been estimated, one can obtain the Cartesian and joint coordinates of the human arm. These are crucial to ensure safe planning of human limb movement in two ways:

1) Restrict the human joint movement to a safe range, which may differ depending on the subject. This requirement is fulfilled by the inverse kinematic model of the human upper limb.
2) Prevent collisions of the human arm with the environment, which is also important for safe planning of the placement motion.

Inverse and forward kinematic models of the human arm in $\mathcal{S}$ can easily be obtained using a geometric approach and are defined by (29) and (30), respectively.

$$\mathbf{q}_h = \begin{bmatrix} \arctan\left(\dfrac{x_{h_G} - l_{h_2}\cos\left(\psi_{h_G}\right)}{y_{h_G} - l_{h_2}\sin\left(\psi_{h_G}\right)}\right) \\ \psi_{h_G} - \arctan\left(\dfrac{x_{h_G} - l_{h_2}\cos\left(\psi_{h_G}\right)}{y_{h_G} - l_{h_2}\sin\left(\psi_{h_G}\right)}\right) \end{bmatrix}, \quad (29)$$

where x_{h_G}, y_{h_G}, and ψ_{h_G} are the elements of $\mathbf{x}_{h_G}$.

$$\mathbf{x}_{h_E} = \begin{bmatrix} l_{h_1}\cos\left(q_{h_1}\right) \\ l_{h_1}\sin\left(q_{h_1}\right) \\ q_{h_1} \end{bmatrix} + \boldsymbol{\Sigma}_{h_S},$$
$$\mathbf{x}_{h_G} = \begin{bmatrix} l_{h_2}\cos\left(q_{h_1} + q_{h_2}\right) \\ l_{h_2}\sin\left(q_{h_1} + q_{h_2}\right) \\ q_{h_1} + q_{h_2} \end{bmatrix} + \mathbf{x}_{h_E}, \quad (30)$$

where l_{h_1} and l_{h_2} are the elements of $\mathbf{l}_h$; q_{h_1} and q_{h_2} are the elements of $\mathbf{q}_h$; and $\mathbf{x}_{h_G}$ and $\mathbf{x}_{h_E}$ are calculated with respect to the reference frame at the shoulder of the human arm $\boldsymbol{\Sigma}_{h_S}$.

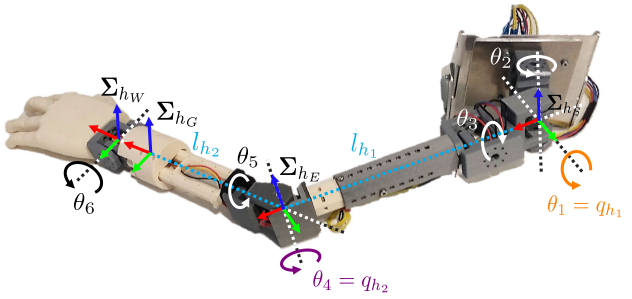

FIGURE 3. A 6-DoF 3D-printed, customizable, and sensorized anthropomorphic arm that simulates the human arm's kinodynamic behavior is used as a dummy for experimental validation of the proposed methodology.

IV. EXPERIMENTS

To evaluate the performance of the proposed approach, ground-truth data, including the actual kinematic parameters of the limbs and the joint value trajectories, must be obtained. For this purpose, a sensorized dummy with configurable lengths and weights is used (see Fig. 3).

A. DUMMY ARM

The core design of the dummy is similar to that of the bones of a human arm. Conceptually, the dummy can be 3D-printed using common FDM 3D-printers. The dummy arm has six DoFs: a three-joint spherical shoulder, a two-joint elbow, and a simplified single-joint wrist. Note that the dummy has 6-DoFs, whereas a human upper-limb has 7-DoFs. The missing dummy DoF corresponds to wrist abduction/adduction. Since the robot grasps the forearm, wrist DoFs do not affect the estimation movement. The dummy's kinematic behavior mimics that of a real human arm, including the joint range of motion. This device is modular as it allows for modifications in the link lengths: links of different lengths can be used to alter the length of the humerus (l_{h1}). A cylindrical ring with a 60*mm* diameter serves as the forearm grasping point, imitating the shape of a human wrist. This ring can be placed at different locations along the "ulna-radius" segment, allowing for modifications in the length l_{h2}. To imitate the dynamic behavior of a human arm, additional weights are attached around the artificial bones. The complete system design is available for download from a public repository.[1]

Analog linear potentiometers built into the six DoFs measure the joint coordinates of the arm, θ_h. An Arduino Mega2560 microcontroller maps the electrical signals to angular values, with a 100 Hz sampling rate. The microcontroller integrates a 10-bit ADC. Hence, the joint angles are measured with a resolution of 0.0047 rad. Because the movements in $\mathcal{S}$ are the only ones considered in this study, only two joints of the arm are observed (see Fig. 3).

B. EXPERIMENT DESIGN

A KUKA iiwa lbr 7R robot is used for the experiments. The impedance controller can be programmed with specific

[1] www.github.com/Taislab/dummyarm

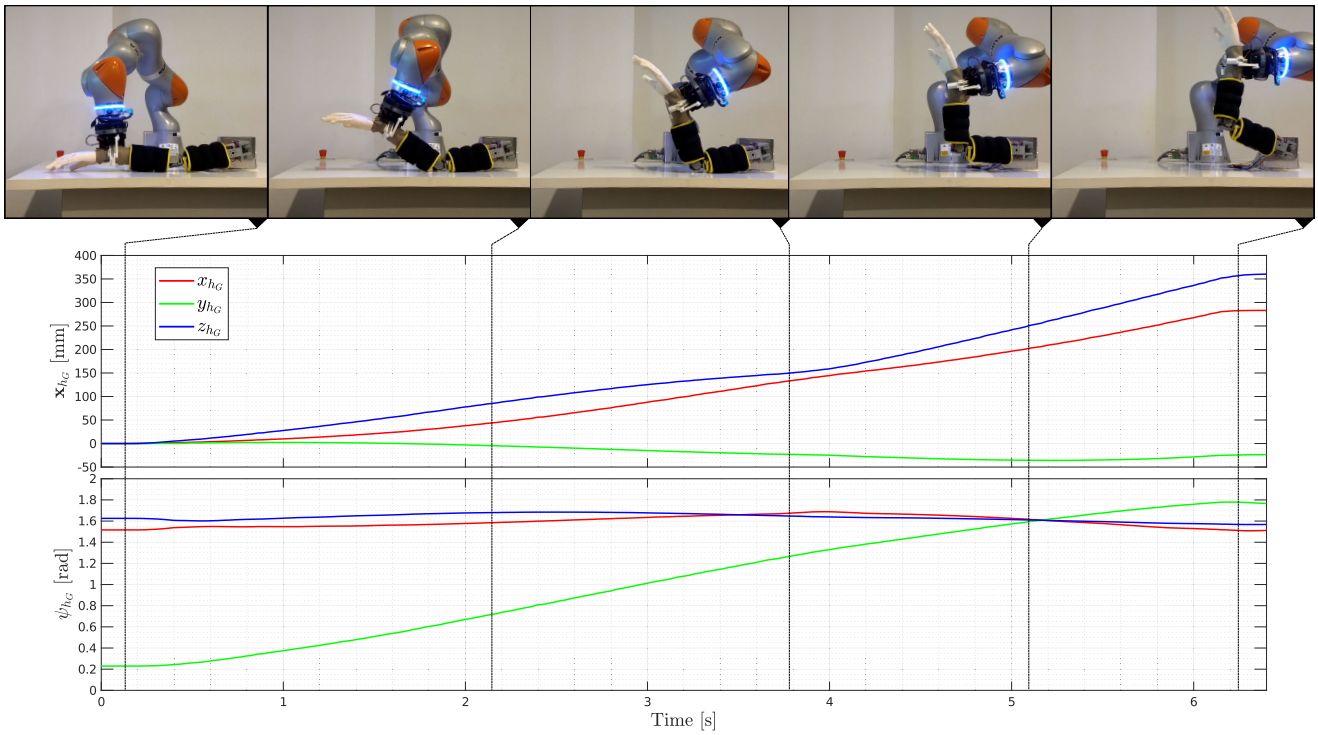

FIGURE 4. Time-lapse of one of the experiments (top), positions (top graph) and orientations (bottom graph) of $\mathbf{x}_{h_G}$ during the execution of one experiment. Although the position deviates a little from $\mathcal{S}$, the predominant motion occurs in $\mathcal{S}$. The same effect can be observed in the orientation, where the most significant change occurs in the axis perpendicular to $\mathcal{S}$ (Y-axis).

Cartesian stiffness $\mathbf{K}_r$ and damping $\mathbf{D}_r$ (q) matrices. $\mathbf{K}_r$ was implemented as a diagonal matrix whose values were chosen to enable a lifting motion of the human arm in $\mathcal{S}$ and simultaneously restrict motion in other directions.

For safety reasons, $\mathbf{D}_r$ $(q,)$ is tuned to provide overdamped behavior. Under such compliant control, the resulting trajectory and forces exerted by the end-effector depend on the interaction wrenches applied by the subject, who, during lifting, is assumed to be passive (i.e., $\tau_h = 0$). Nevertheless, additional safety measures are included in the robot controller to ensure safe manipulation, even when the subject plays an active role in the task: the velocity of the robot is limited to 2.5% of the maximum reachable speed to minimize the risk of injury and the maximum force that the robot can exert and the Cartesian workspace are constrained. Thus, the robot cannot exceed the natural range of motion of human joints.

Six experiments are performed using the same link weights ($m_1 = 1.55$ kg, $m_2 = 1.317$ kg) but different lengths. With the dummy shoulder fixed to the table, the robot is guided manually to $\mathbf{x}_{h_G}$. Once the wrist is grasped, the manipulator follows the trajectory specified in Section III-A. As the grasping point is the only known point, all computations and measurements are performed with reference to this point. During the experiments, end-effector Cartesian pose and dummy joint position data are collected. All measurements are recorded at a sampling rate of 100 Hz. For simplicity, the $\mathcal{S}$ plane and the XZ plane of the robot reference framework are defined as parallel.

V. RESULTS AND DISCUSSION

The estimation trajectory performed by the robot is shown in Fig. 4. The sequence of images at the top, which illustrates the experimental process, was recorded as a video.[2] The Cartesian trajectory in terms of position (graph at the top) and orientation (graph at the bottom) of $\mathbf{x}_{h_G}$ are also shown. The motion is not perfectly constrained to the $\mathcal{S}$-plane; some divergence from the plane is observed. Nevertheless, the main component of the motion is contained in $\mathcal{S}$, so the simplifications of the model of the human arm made in Section II-B are valid.

The performance of the proposed methodology is evaluated by comparing the ground-truth and estimated trajectories. The outcomes are shown in Fig. 5, where the top plot represents the Cartesian trajectory of the elbow. The estimated X and Z coordinates are represented by dashed and dotted lines for estimations performed by HT and LS, respectively, whereas the ground-truth data are represented by continuous lines. The plot at the bottom presents the trajectories of the two joints of the dummy arm.

Fig. 6 presents plots of the Cartesian paths in $\mathcal{S}$ for the six experiments. These graphs show that the HT-estimated, LS-estimated and ground-truth elbow positions, marked with circles, asterisks and crosses, respectively, follow similar trajectories. The predicted shoulder positions, marked with a triangle and a diamond for HT and LS, respectively, present

[2]https://youtu.be/cNCqYyKOUVM

TABLE 1. Summary of the results: Ground-truth and estimated lengths and mean (μ) and standard deviation (σ) of the RMSE of joints and Cartesian positions. For each experiment, the results obtained with HT and LS are presented at the top and bottom of each cell, respectively, for easy comparison. *Note: The Cartesian position of the shoulder was estimated only once; hence, the standard deviation is 0.

Exp.	l_{h1}	l_{h2}	l_{h1}^{HT} l_{h1}^{LS}	l_{h2}^{HT} l_{h2}^{LS}	$\mu_{q_{h_1}}^{HT}$ $\mu_{q_{h_1}}^{LS}$	$\sigma_{q_{h_1}}^{HT}$ $\sigma_{q_{h_1}}^{LS}$	$\mu_{q_{h_2}}^{HT}$ $\mu_{q_{h_2}}^{LS}$	$\sigma_{q_{h_2}}^{HT}$ $\sigma_{q_{h_2}}^{LS}$	$\mu_{\Sigma_{h_E}}^{HT}$ $\mu_{\Sigma_{h_E}}^{LS}$	$\sigma_{\Sigma_{h_E}}^{HT}$ $\sigma_{\Sigma_{h_E}}^{LS}$	$\mu_{\Sigma_{h_S}}^{HT}$ $\mu_{\Sigma_{h_S}}^{LS}$	$\sigma_{\Sigma_{h_S}}^{HT*}$ $\sigma_{\Sigma_{h_S}}^{LS*}$
1	330	200	339 333.25	199 216.12	$1.3402e^{-2}$ $1.6798e^{-02}$	$6.0851e^{-3}$ $5.8873e^{-3}$	$1.9497e^{-2}$ $4.4404e^{-2}$	$9.3472e^{-3}$ $2.1118e^{-2}$	4.0753 16.387	2.3270 4.0623	11.264 13.021	0 0
2	330	180	335 302.45	179 212.99	$5.9380e^{-3}$ $6.5370e^{-2}$	$4.0687e^{-3}$ $2.9497e^{-2}$	$1.9825e^{-2}$ $5.8048e^{-2}$	$1.6693e^{-2}$ $2.9705e^{-2}$	3.3758 25.450	1.7417 8.9402	7.1496 23.070	0 0
3	300	200	312 295.57	199 219.78	$1.8420e^{-2}$ $5.1236e^{-2}$	$7.0118e^{-3}$ $1.8237e^{-2}$	$3.4763e^{-2}$ $6.7021e^{-2}$	$1.6734e^{-2}$ $2.9390e^{-2}$	2.5047 15.207	1.6050 5.5080	12.994 3.2653	0 0
4	300	180	309 277.93	178 199.79	$2.2668e^{-2}$ $6.7885e^{-2}$	$6.7438e^{-3}$ $2.9639e^{-2}$	$2.3956e^{-2}$ $5.8383e^{-2}$	$1.5699e^{-2}$ $3.0305e^{-2}$	6.3777 12.849	3.3123 4.8660	15.494 21.452	0 0
5	270	200	282 260.77	200 215.91	$8.4200e^{-3}$ $4.3893e^{-2}$	$5.6806e^{-3}$ $1.8253e^{-2}$	$2.7097e^{-2}$ $6.8209e^{-2}$	$1.9907e^{-2}$ $2.3381e^{-2}$	4.3389 15.292	1.3903 4.9043	10.553 9.7634	0 0
6	270	180	297 268.91	174 198.33	$1.7938e^{-2}$ $3.2628e^{-2}$	$7.2856e^{-3}$ $1.7046e^{-2}$	$3.0464e^{-2}$ $7.0260e^{-2}$	$2.3413e^{-2}$ $2.6840e^{-2}$	10.531 10.091	5.2771 4.2329	24.511 2.1565	0 0

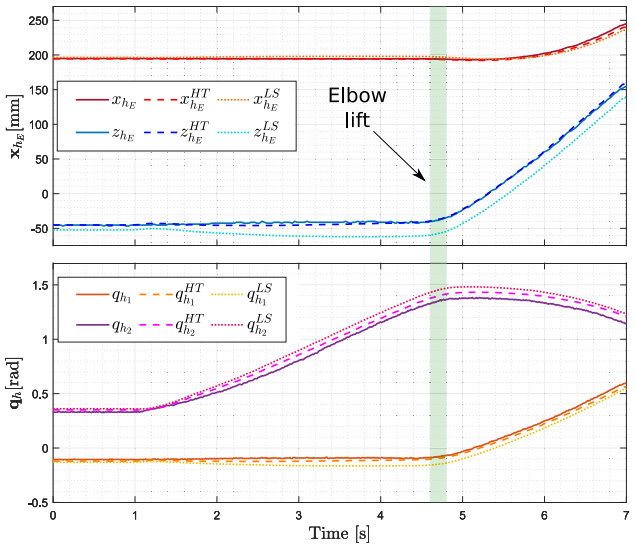

FIGURE 5. Ground-truth and estimated Cartesian trajectories (top) and joint trajectories (bottom) for the elbow in one experiment. The green region indicates the time at which the elbow starts to lift.

more substantial estimation error. This is due to the estimation process: as described in Section III-C, the proposed method first estimates the pose of the elbow, $\tilde{\mathbf{x}}_{h_E}$; then, $\tilde{\mathbf{x}}_{h_E}$ is used to estimate the pose of the shoulder, $\tilde{\mathbf{x}}_{h_S}$. Thus, $\tilde{\mathbf{x}}_{h_S}$ includes the accumulated errors of both the elbow and shoulder estimates.

Table 1 presents a summary of the results, including the actual and estimated link lengths for each experiment and the estimation errors. Between the length estimations ($\tilde{l}_{h_1}$ and $\tilde{l}_{h_2}$), the former exhibits a lower error than the latter owing to the aforementioned accumulation error. The same effect is observed for shoulder estimation, which is performed from $\tilde{l}_{h1}$. The joint and Cartesian estimation errors are represented by the mean value and the standard deviation of the root-mean-square-error (RMSE) function. The error accumulation effects are more prominent in the elbow and shoulder pose estimations. As expected, the elbow positions exhibit lower errors than do the shoulder positions. Compared with LS, HT is better able to handle nonlocality and is more robust to noise, as noisy points are unlikely to contribute to a single cell. In terms of computational complexity, the time needed for the estimation varies with the number of points recorded during the motion. For a path of 300 points, HT takes 1.7334 seconds, whereas LS takes 0.0051 seconds using an Intel Core i7-3630 computer with 8GB of RAM. Considering the process followed by each method (Section III-C), it is clear that HT is more complex than LS, but the difference in time is also explained by differences in implementation. For LS, we used the *MatLab Curve Fitting Toolbox*, which provides highly optimized algorithms for regression and parameter estimation. By contrast, HT was implemented from scratch. The implementation of HT is not complicated, as only three parameters are considered, but the generated code has not been optimized. Even though HT takes almost 2 seconds to complete the estimation, it is sufficiently fast to not interfere with a possible rehabilitation task. The results confirm the initial hypothesis: HT is a highly suitable method to identify any circumference present in the path, such as that followed by the wrist during the identification of the trajectory. Despite the accumulated error, the estimated position of the upper arm is highly accurate, with an error of less than 1 cm.

Based on these results, it can be concluded that the proposed method functioned appropriately. The method is capable of estimating kinematic models of human upper limbs without the use of external sensors. Therefore, the results demonstrate that the proposed methodology can be used as a preparatory step in rehabilitation and assistive applications in which the human arm kinematic model must be accurately defined. Nevertheless, a few assumptions were incorporated in this study, which limits the applicability of the proposed method to specific real-world tasks.

As previously discussed, robotic manipulation of human limbs is exceptionally complicated and represents a significant challenge in robotics. Multiple aspects related to robotic control, manipulation, artificial intelligence, and physical interaction are yet to be considered; hence, although the proposed methodology offers high accuracy, it has certain limitations with respect to real-world applications. The first assumption is that the subject's arm is on a surface and that the available motions are limited to the sagittal plane. Although

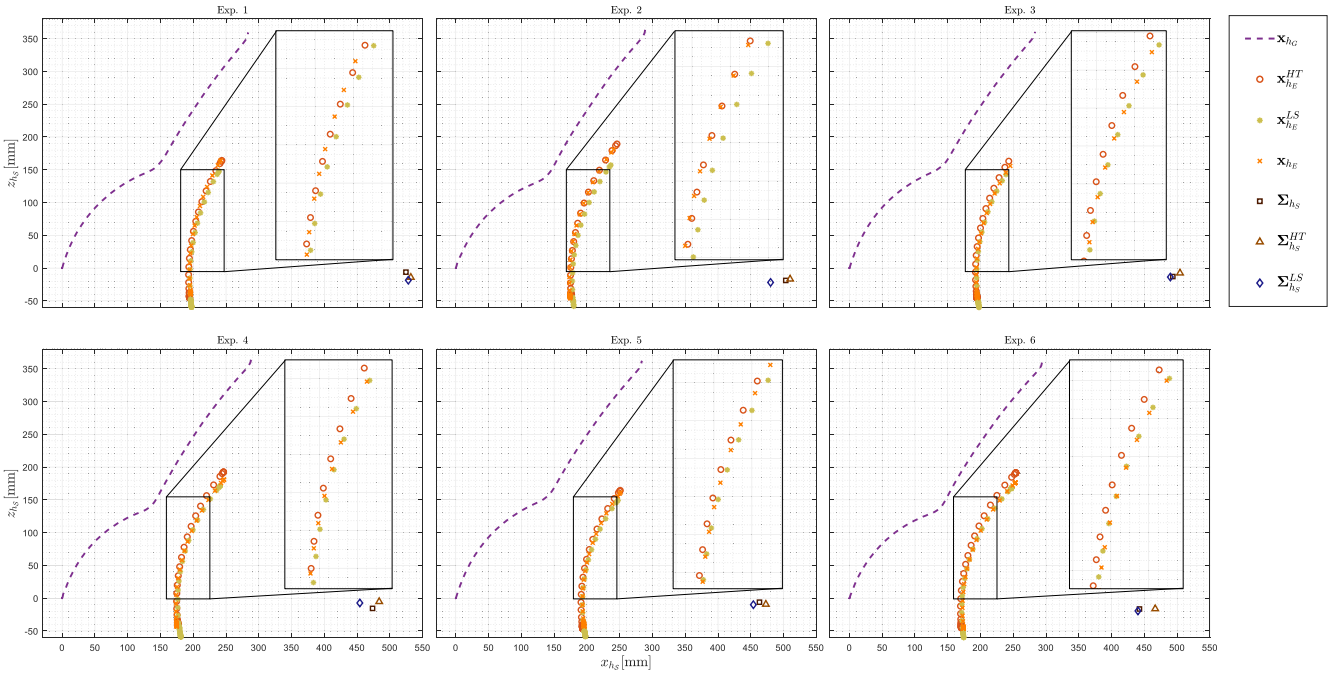

FIGURE 6. Graphical representation of the results obtained for the six experiments in the $\mathcal{S}$ plane. For each point of the Cartesian path (purple dotted line), the proposed method estimates the positions of the elbow and shoulder of the dummy arm. The circles and squares represent the actual positions of the dummy's elbow and shoulder, respectively. The crosses and triangles represent the elbow and shoulder positions estimated by HT, while the asterisks and diamonds represent the elbow and shoulder positions estimated by LS, respectively. The squared area represents a zoomed in view of the elbow paths to illustrate the differences between the real trajectory and the trajectories estimated by HT and LS.

our experiments were conducted under this assumption, the proposed method can be extended to different human postures in the sagittal plane. The subject can also stand or sit as long as the arm and the estimation motion remain in the sagittal plane, with the elbow initially lying on a surface. Nevertheless, to incorporate such postures, the motion planner must be modified, and a new identification path must be defined.

Second, the subject is considered passive during the parameter estimation. This condition must be fulfilled for correct functioning of the method. If the subject resists the robot, the considerations discussed in Section II will not be fulfilled. Consequently, the trajectory during the estimation phase may present an erratic shape, and the method may fail. Because of the passive-subject assumption, the human shoulder is considered stationary, that is, it occupies a fixed position in space. This is true when the robot manipulates the human limb under the action of a proper planner. Finally, the method is restricted to the sagittal plane, $\mathcal{S}$. This is the most significant limitation of the method and must be overcome.

The main safety risks involved in robotic manipulation of human limbs include exceeding the joint limits, causing pain or injuries, and collisions with the environment or other body parts. The use of low velocity profiles and impedance control can help minimize range violations and incidences of hitting a surface with the elbow. However, safety cannot be ensured without proper planning. Motion planning can be performed whenever a model of the human arm is available. Methods for collision-free planning and task-space boundaries used in robotics can be applied.

VI. CONCLUSION

This paper presented a method for estimating human arm parameters via robotic manipulation. The estimation method utilizes the kinesthetic information of the robot, which moves along a compliant trajectory that can easily be modified based on human arm kinodynamics. The lengths of the links, the joints, and the Cartesian positions of the human arm model were obtained by applying the Hough transform to measurements from the robot's position sensors. To evaluate the accuracy of the method, six experiments with different arm lengths were conducted utilizing a sensorized dummy that provided ground-truth measurements. The experimental results demonstrate the effectiveness of the proposed methodology in terms of human arm pose estimation and safe manipulation.

However, safe manipulation requires specific considerations and depends on the desired task. Hence, the implementation of safe manipulation levels will be further studied for different potential applications, such as elderly care and rehabilitation. In addition, additional safety parameters, such as joint ranges and maximum joint velocities and torques, must be considered in motion planning after the estimation.

Moreover, the absence of calibration processes makes the proposed method a ready-to-use solution, even for nonspecialized personnel. The method only requires manually placing the robot at the grasping point and executing the estimation program. In addition, the method offers a generality unseen in the majority of rehabilitation systems. In contrast to existing exoskeletons, our system can be used for any patient without customization.

In conclusion, the use of a commercial robot manipulator and the presence of only minor errors in the estimation process make the proposed method an excellent alternative to vision-based estimation systems. Although the proposed method has some limitations (constraints of the sagittal plane and offline parameter estimation), it highlights the importance of kinesthetic information. In addition, once the kinematic parameters are estimated, they can be used not only for online tasks but also to detect undesirable behavior during human arm manipulation. The main advantages of this method are its plug-and-play orientation, improved accuracy compared with that of vision-based methods, and reduced cost and complexity compared with those of noncommercial, bulky exoskeleton-based systems.

Furthermore, this work opens the door to future research in the unexplored field of robotic manipulation of human limbs. Future studies could consider implementing an extended version of the proposed methodology to work beyond the sagittal plane. This approach could also be applied to estimate the dynamics of the human arm during pHRI tasks. In addition, the proposed method will be considered for practical applications with real humans. In this regard, a generalization of the proposed method is desired for use with humans of different complexion.

REFERENCES

[1] D. Feil-Seifer and M. J. Mataric, "Defining socially assistive robotics," in *Proc. Int. Conf. Rehabil. Robot. (ICORR)*, 2005, pp. 465–468.

[2] T. Bhattacharjee, G. Lee, H. Song, and S. S. Srinivasa, "Towards robotic feeding: Role of haptics in fork-based food manipulation," *IEEE Robot. Autom. Lett.*, vol. 4, no. 2, pp. 1485–1492, Apr. 2019.

[3] Z. Erickson, M. Collier, A. Kapusta, and C. C. Kemp, "Tracking human pose during robot-assisted dressing using single-axis capacitive proximity sensing," *IEEE Robot. Autom. Lett.*, vol. 3, no. 3, pp. 2245–2252, Jul. 2018.

[4] I. Carrera, H. A. Moreno, R. Saltarén, C. Pérez, L. Puglisi, and C. Garcia, "Road: Domestic assistant and rehabilitation robot," *Med. Biol. Eng. Comput.*, vol. 49, no. 10, p. 1201, 2011.

[5] J. M. Gandarias, F. Pastor, A. J. Muñoz-Ramírez, A. J. García-Cerezo, and J. M. Gómez-de-Gabriel, "Underactuated gripper with forearm roll estimation for human limbs manipulation in rescue robotics," in *Proc. IEEE/RSJ Int. Conf. Intell. Robots Syst. (IROS)*, Nov. 2019, pp. 5937–5942.

[6] L. Peternel, W. Kim, J. Babič, and A. Ajoudani, "Towards ergonomic control of human-robot co-manipulation and handover," in *Proc. IEEE-RAS 17th Int. Conf. Humanoid Robot. (Humanoids)*, Nov. 2017, pp. 55–60.

[7] A. J. Westerveld, B. J. Aalderink, W. Hagedoorn, M. Buijze, A. C. Schouten, and H. V. D. Kooij, "A damper driven robotic endpoint manipulator for functional rehabilitation exercises after stroke," *IEEE Trans. Biomed. Eng.*, vol. 61, no. 10, pp. 2646–2654, Oct. 2014.

[8] A. Basteris, S. M. Nijenhuis, A. H. Stienen, J. H. Buurke, G. B. Prange, and F. Amirabdollahian, "Training modalities in robot-mediated upper limb rehabilitation in stroke: A framework for classification based on a systematic review," *J. NeuroEng. Rehabil.*, vol. 11, no. 1, p. 111, 2014.

[9] B. R. Brewer, S. K. McDowell, and L. C. Worthen-Chaudhari, "Poststroke upper extremity rehabilitation: A review of robotic systems and clinical results," *Topics Stroke Rehabil.*, vol. 14, no. 6, pp. 22–44, Dec. 2007.

[10] G. Sprint, D. J. Cook, D. L. Weeks, and V. Borisov, "Predicting functional independence measure scores during rehabilitation with wearable inertial sensors," *IEEE Access*, vol. 3, pp. 1350–1366, 2015.

[11] A. Pennycott, D. Wyss, H. Vallery, V. Klamroth-Marganska, and R. Riener, "Towards more effective robotic gait training for stroke rehabilitation: A review," *J. NeuroEng. Rehabil.*, vol. 9, no. 1, p. 65, 2012.

[12] H. I. Krebs, J. J. Palazzolo, L. Dipietro, M. Ferraro, J. Krol, K. Rannekleiv, B. T. Volpe, and N. Hogan, "Rehabilitation robotics: Performance-based progressive robot-assisted therapy," *Autonom. Robot.*, vol. 15, no. 1, pp. 7–20, Jul. 2003.

[13] L. Peternel, N. Tsagarakis, and A. Ajoudani, "A human–robot co-manipulation approach based on human sensorimotor information," *IEEE Trans. Neural Syst. Rehabil. Eng.*, vol. 25, no. 7, pp. 811–822, Jul. 2017.

[14] L. Bi and C. Guan, "A review on EMG-based motor intention prediction of continuous human upper limb motion for human-robot collaboration," *Biomed. Signal Process. Control*, vol. 51, pp. 113–127, May 2019.

[15] W. Kim, P. Balatti, E. Lamon, and A. Ajoudani, "MOCA-MAN: A MObile and reconfigurable collaborative robot assistant for conjoined huMAN-robot actions," in *Proc. IEEE Int. Conf. Robot. Autom. (ICRA)*, May 2020, pp. 10191–10197.

[16] E. Rocon, J. M. Belda-Lois, A. F. Ruiz, M. Manto, J. C. Moreno, and J. L. Pons, "Design and validation of a rehabilitation robotic exoskeleton for tremor assessment and suppression," *IEEE Trans. Neural Syst. Rehabil. Eng.*, vol. 15, no. 3, pp. 367–378, Sep. 2007.

[17] M. Lazzaroni, S. Toxiri, D. G. Caldwell, S. Anastasi, L. Monica, E. D. Momi, and J. Ortiz, "Acceleration-based assistive strategy to control a back-support exoskeleton for load handling: Preliminary evaluation," in *Proc. IEEE 16th Int. Conf. Rehabil. Robot. (ICORR)*, Jun. 2019, pp. 625–630.

[18] C. N. Schabowsky, S. B. Godfrey, R. J. Holley, and P. S. Lum, "Development and pilot testing of HEXORR: Hand EXOskeleton rehabilitation robot," *J. NeuroEng. Rehabil.*, vol. 7, no. 1, p. 36, 2010.

[19] E. Pezent, C. G. Rose, A. D. Deshpande, and M. K. O'Malley, "Design and characterization of the OpenWrist: A robotic wrist exoskeleton for coordinated hand-wrist rehabilitation," in *Proc. Int. Conf. Rehabil. Robot. (ICORR)*, Jul. 2017, pp. 720–725.

[20] B. Sheng, S. Xie, L. Tang, C. Deng, and Y. Zhang, "An industrial robot-based rehabilitation system for bilateral exercises," *IEEE Access*, vol. 7, pp. 151282–151294, 2019.

[21] P. Balatti, F. Fusaro, N. Villa, E. Lamon, and A. Ajoudani, "A collaborative robotic approach to autonomous pallet jack transportation and positioning," *IEEE Access*, vol. 8, pp. 142191–142204, 2020.

[22] E. Lamon, F. Fusaro, P. Balatti, W. Kim, and A. Ajoudani, "A visuo-haptic guidance interface for mobile collaborative robotic assistant (MOCA)," in *Proc. IEEE/RSJ Int. Conf. Intell. Robots Syst. (IROS)*, Oct. 2020, pp. 11253–11260.

[23] P. Araujo-Gómez, V. Mata, M. Díaz-Rodríguez, A. Valera, and A. Page, "Design and kinematic analysis of a novel 3UPS/RPU parallel kinematic mechanism with 2T2R motion for knee diagnosis and rehabilitation tasks," *J. Mech. Robot.*, vol. 9, no. 6, pp. 061004-1–061004-10, Dec. 2017.

[24] M. Abbasi and A. Afsharfard, "Modeling and experimental study of a hand tremor suppression system," *Mechanism Mach. Theory*, vol. 126, pp. 189–200, Aug. 2018.

[25] M. Vallés, J. Cazalilla, Á. Valera, V. Mata, Á. Page, and M. Díaz-Rodríguez, "A 3-PRS parallel manipulator for ankle rehabilitation: Towards a low-cost robotic rehabilitation," *Robotica*, vol. 35, no. 10, p. 1939–1957, 2017.

[26] Z. Cao, G. Hidalgo, T. Simon, S.-E. Wei, and Y. Sheikh, "OpenPose: Realtime multi-person 2D pose estimation using part affinity fields," *IEEE Trans. Pattern Anal. Mach. Intell.*, vol. 43, no. 1, pp. 172–186, Jan. 2021.

[27] W. Ren, O. Ma, H. Ji, and X. Liu, "Human posture recognition using a hybrid of fuzzy logic and machine learning approaches," *IEEE Access*, vol. 8, pp. 135628–135639, 2020.

[28] A. Lioulemes, M. Theofanidis, V. Kanal, K. Tsiakas, M. Abujelala, C. Collander, W. B. Townsend, A. Boisselle, and F. Makedon, "MAGNI dynamics: A vision-based kinematic and dynamic upper-limb model for intelligent robotic rehabilitation," *Int. J. Biomed. Biol. Eng.*, vol. 11, no. 4, pp. 158–167, 2017.

[29] G. A. Farulla, D. Pianu, M. Cempini, M. Cortese, L. Russo, M. Indaco, R. Nerino, A. Chimienti, C. Oddo, and N. Vitiello, "Vision-based pose estimation for robot-mediated hand telerehabilitation," *Sensors*, vol. 16, no. 2, p. 208, Feb. 2016.

[30] D. Phan, B. Kashyap, P. N. Pathirana, and A. Seneviratne, "A constrained nonlinear optimization solution for 3D orientation estimation of the human limb," in *Proc. 10th Biomed. Eng. Int. Conf. (BMEiCON)*, Aug. 2017, pp. 1–4.

[31] A. Atrsaei, H. Salarieh, and A. Alasty, "Human arm motion tracking by orientation-based fusion of inertial sensors and Kinect using unscented Kalman filter," *J. Biomech. Eng.*, vol. 138, no. 9, pp. 091005-1–091005-13, Sep. 2016.

[32] F. Just, Ö. Özen, S. Tortora, V. Klamroth-Marganska, R. Riener, and G. Rauter, "Human arm weight compensation in rehabilitation robotics: Efficacy of three distinct methods," *J. NeuroEng. Rehabil.*, vol. 17, no. 1, pp. 1–17, Dec. 2020.

[33] M. Laitenberger, M. Raison, D. Périé, and M. Begon, "Refinement of the upper limb joint kinematics and dynamics using a subject-specific closed-loop forearm model," *Multibody Syst. Dyn.*, vol. 33, no. 4, pp. 413–438, Apr. 2015.
[34] J. Gandarias, J. Gómez-de-Gabriel, and A. García-Cerezo, "Enhancing perception with tactile object recognition in adaptive grippers for human–robot interaction," *Sensors*, vol. 18, no. 3, p. 692, Feb. 2018.
[35] L. Liu, J. Ma, Y. Luo, and H. Wu, "Mechanism design and kinematics analysis of multifunctional waist rehabilitation bed," *Vibroengineering PROCEDIA*, vol. 22, pp. 194–199, Mar. 2019, doi: 10.21595/vp.2019.20539.
[36] P. Piraintorn and V. Sa-Ing, "Stroke rehabilitation based on intelligence interaction system," in *Proc. 17th Int. Conf. Electr. Eng./Electron., Comput., Telecommun. Inf. Technol. (ECTI-CON)*, Jun. 2020, pp. 648–651.
[37] Y. Ren, Y.-N. Wu, C.-Y. Yang, T. Xu, R. L. Harvey, and L.-Q. Zhang, "Developing a wearable ankle rehabilitation robotic device for in-bed acute stroke rehabilitation," *IEEE Trans. Neural Syst. Rehabil. Eng.*, vol. 25, no. 6, pp. 589–596, Jun. 2017.
[38] J. R. Medina, T. Lorenz, and S. Hirche, "Considering human behavior uncertainty and disagreements in human–robot cooperative manipulation," in *Trends in Control and Decision-Making for Human–Robot Collaboration Systems*, Y. Wang and F. Zhang, Eds. Cham, Switzerland: Springer, 2017, pp. 207–240.
[39] G. Averta, D. Caporale, C. Della Santina, A. Bicchi, and M. Bianchi, "A technical framework for human-like motion generation with autonomous anthropomorphic redundant manipulators," in *Proc. IEEE Int. Conf. Robot. Autom. (ICRA)*, May 2020, pp. 3853–3859.
[40] J. M. Gómez-de-Gabriel, J. M. Gandarias, F. J. Pérez-Maldonado, F. J. García-Núñcz, E. J. Fernández-García, and A. J. García-Cerezo, "Methods for autonomous wristband placement with a search-and-rescue aerial manipulator," in *Proc. IEEE/RSJ Int. Conf. Intell. Robots Syst. (IROS)*, Oct. 2018, pp. 7838–7844.
[41] F. Ozkul and D. E. Barkana, "Upper-extremity rehabilitation robot RehabRoby: Methodology, design, usability and validation," *Int. J. Adv. Robotic Syst.*, vol. 10, no. 12, p. 401, Dec. 2013.
[42] R. O. Duda and P. E. Hart, "Use of the Hough transformation to detect lines and curves in pictures," *Commun. ACM*, vol. 15, no. 1, pp. 11–15, Jan. 1972.
[43] S. Jung, T. C. Hsia, and R. G. Bonitz, "Force tracking impedance control of robot manipulators under unknown environment," *IEEE Trans. Control Syst. Technol.*, vol. 12, no. 3, pp. 474–483, May 2004.
[44] O. Khatib, "A unified approach for motion and force control of robot manipulators: The operational space formulation," *IEEE J. Robot. Autom.*, vol. JRA-3, no. 1, pp. 43–53, Feb. 1987.
[45] F. Ficuciello, A. Romano, L. Villani, and B. Siciliano, "Cartesian impedance control of redundant manipulators for human-robot co-manipulation," in *Proc. IEEE/RSJ Int. Conf. Intell. Robots Syst.*, Sep. 2014, pp. 2120–2125.
[46] C. Ott, *Cartesian Impedance Control of Redundant and Flexible-Joint Robots*. Berlin, Germany: Springer, 2008.
[47] A. Albu-Schaffer, C. Ott, U. Frese, and G. Hirzinger, "Cartesian impedance control of redundant robots: Recent results with the DLR-light-weight-arms," in *Proc. IEEE Int. Conf. Robot. Autom. (ICRA)*, vol. 3, Sep. 2003, pp. 3704–3709.
[48] S. Chatterjee and A. S. Hadi, *Regression Analysis by Example*. Hoboken, NJ, USA: Wiley, 2015.
[49] J. Illingworth and J. Kittler, "A survey of the Hough transform," *Comput. Vis., Graph., Image Process.*, vol. 44, no. 1, pp. 87–116, 1988.
[50] M. Gautier and P. Poignet, "Extended Kalman filtering and weighted least squares dynamic identification of robot," *Control Eng. Pract.*, vol. 9, no. 12, pp. 1361–1372, Dec. 2001. [Online]. Available: https://www.sciencedirect.com/science/article/pii/S0967066101001058
[51] B. L. Bonilla and H. H. Asada, "A robot on the shoulder: Coordinated human-wearable robot control using coloured Petri nets and partial least squares predictions," in *Proc. IEEE Int. Conf. Robot. Autom. (ICRA)*, May 2014, pp. 119–125.
[52] A. Wan, J. Xu, H. Chen, S. Zhang, and K. Chen, "Optimal path planning and control of assembly robots for hard-measuring easy-deformation assemblies," *IEEE/ASME Trans. Mechatronics*, vol. 22, no. 4, pp. 1600–1609, Aug. 2017.
[53] V. Strejc, "Least squares parameter estimation," *Automatica*, vol. 16, no. 5, pp. 535–550, 1980. [Online]. Available: https://www.sciencedirect.com/science/article/pii/0005109880900771
[54] S. Boyd and L. Vandenberghe, *Introduction to Applied Linear Algebra: Vectors, Matrices, and Least Squares*. Cambridge, U.K.: Cambridge Univ. Press, 2018.

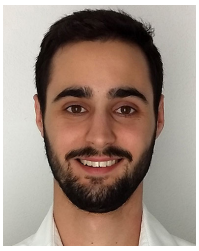

FRANCISCO J. RUIZ-RUIZ received the B.S. and M.S. degrees in mechatronics engineering from the University of Málaga, Málaga, Spain, in 2018 and 2019, respectively, where he is currently pursuing the Ph.D. degree in mechatronics engineering. He is also a Research Assistant with the Department of Systems Engineering and Automation, University of Málaga. His research interests include pHRI, control design of robotic manipulators, and the Internet of Things.

JUAN M. GANDARIAS (Member, IEEE) received the B.S., M.S., and Ph.D. degrees in mechatronics from the University of Málaga, in 2015, 2017, and 2020, respectively. He is a Postdoctoral Researcher with the Human-Robot Interfaces and Physical Interaction Lab (HRI2), Istituto Italiano di Tecnologia (IIT). He has contributed to several Spanish and European projects related to search-and-rescue, physical robotic assistance and human–robot collaboration in industrial environments. His research interests include pHRI, human modeling, and haptic perception.

FRANCISCO PASTOR received the M.Sc. degree in mechatronics engineering from the University of Málaga, Spain, in 2017. He is currently pursuing the Ph.D. degree in mechatronics engineering with the Robotics and Mechatronics Group, University of Málaga. He has collaborated as a Researcher in a project on rescue robotics and mobile robots. His current research interests include pHRI and tactile perception.

JESÚS M. GÓMEZ-DE-GABRIEL (Member, IEEE) received the Engineering and Ph.D. degrees in computer science from the University of Málaga, Málaga, Spain, in 1990 and 1999, respectively. He is currently an Associate Professor with the Department of Systems Engineering and Automation, University of Málaga. He has led a project on telerobotic surgery and has participated in medical robotics projects and other projects related to mobile robots and factory automation. His current research interests include pHRI, the Internet of Things, education in engineering, and mobile robotics.